Position and Velocity Estimation of a Non-cooperative Source From Asynchronous Packet Arrival Time Measurements

This article has been accepted for publication in a future issue of this journal, but has not been fully edited. Content may change prior to final publication. Citation information: DOI 10.1109/TMC.2018.2792443, IEEE Transactions on Mobile Computing

Position and Velocity Estimation of a Non-cooperative Source From Asynchronous Packet Arrival Time Measurements

Fabio Ricciato, Savio Sciancalepore, Francesco Gringoli, Niccolo Facchi, Gennaro Boggia

Index Terms—Asynchronous Localisation, Opportunistic Localisation, Time of Arrival, Time-Difference of Arrival, Source Localisation

Abstract—We tackle the problem of identifying the trajectory of a moving radio source from Time of Arrival (TOA) measurements collected by a set of cooperating receivers. The considered system is completely asynchronous: nodes clocks are affected by unknown time and frequency offsets, and no control is exerted over packet transmission times. In the proposed solution, the receiver clock offset terms are estimated from TOA measurements on packets originated by non-cooperative reference transmitters, possibly but not necessarily coincidental with reference receivers. Transmission time ambiguity is resolved by exploiting the redundancy associated to the reception of the same packet at multiple receivers. A distinguishing feature of the proposed solution is that it seeks to identify the parameters of the trajectory as a whole, rather than the individual points of transmission as done in traditional point-based approaches. This allows the effective exploitation of TOA measurements collected in lossy scenarios, where the generic packet is received by a smaller subset of the available receivers (at least two). For the problem at hand, we provide distinct estimators based on TOA and Time-Difference of Arrival (TDOA) and prove their equivalence. Numerical results from simulations and from a real WiFi testbed are provided to validate the effectiveness of the proposed method.

1 Introduction

We tackle the problem of passively identifying the trajectory of a moving radio source from Time of Arrival (TOA) measurements collected by a set of cooperating receivers. In order to facilitate practical adoption and minimise cost of deployment, we keep the system-level requirements down at a minimum. In the considered scenario, receiver nodes' clocks are left unsynchronised, and no assumption is made about transmission times, thus enabling the exploitation of signals of opportunity from non-cooperative transmitters.

The general reference scenario is depicted in Fig. 1(a). We consider a wireless system with a blind node transmitting a sequence of packets while moving linearly at constant velocity. In parallel, a set of fixed reference transmitters in known positions are also transmitting. Both types of packets (from the moving blind node and from the fixed reference transmitters) are sent at arbitrary (unknown) transmission times. A set of receivers in fixed known positions overhear and timestamp each received packet, and these data are shared with a central entity in charge of the computation. The problem is to determine the (final) *position* and the *velocity* vector of the blind node from the measured timestamps.

A batch processing approach is considered, where all measurements collected within the last observation window of duration T are jointly processed in a single run to estimate the trajectory parameters (final position and velocity) *with no prior knowledge about the initial node state*. This problem represents the generalisation to a moving node of the classical localisation problem for a static node and was termed "*tracing*[1]" in [1].

The considered system is completely asynchronous and is characterised by the following features:

(a) Receivers are asynchronous: each node clock is affected by unknown *time offset* and *frequency offset*.
(b) Packet transmissions are asynchronous: no explicit control is exerted on the transmission times.
(c) Transmission times are unknown: the tracing process relies exclusively on *reception* timestamps.
(d) The blind node moves with unknown constant velocity.

We highlight that, owing to (b) and (c), transmitters are not required to cooperate explicitly with the tracing process. This is a key aspect of the considered system, as it allows to exploit opportunistically the packets transmitted for communication purposes. A minimum level of cooperation is assumed solely between the (fixed) receivers for the purpose of sharing the collected measurements. We remark that in this scenario the blind node acts purely as transmitter and does not participate to the localisation process.

- *F. Ricciato is with the Faculty of Computer and Information Science, University of Ljubljana, Slovenia. E-mail: fabio.ricciato@fri.uni-lj.si.*
- *S. Sciancalepore and G. Boggia. are with DEI, Dept. of Electrical and Information Engineering, Politecnico di Bari, Italy. E-mail: name.surname@poliba.it.*
- *F. Gringoli is with DII, Dept. of Information Engineering, University of Brescia, Italy. E-mail: francesco.gringoli@unibs.it.*
- *N. Facchi is with Univ. of Trento, Italy. He was with Univ. of Brescia when this work was performed.*

1. The *tracing* problem should be distinguished from the *tracking* problem, where the *current* instantaneous position of the blind node is iteratively updated upon arrival of a new measurement, starting from an initial state that is known at least approximately.

One limitation of the solution elaborated in this paper is reliance on Line-of-Sight (LOS) propagation. This limits its applicability to open outdoor environments. Possible application domains include WiFi based pedestrian tracking [2], people localisation at mass events [3], cattle localisation, WiFi based low-cost sensor networks [4], intrusion detection [5], vehicular localisation [6]. A particular promising application domain is passive drone localisation based on their WiFi signals.

One of the key contributions of our work is to show that the mere set of time-of-arrival (TOA) measurements available at the receivers are sufficient to resolve the many unknown terms that are involved by the adoption of minimalistic system assumptions (a)-(d), namely packet transmission times, clock offsets, clock drifts, node velocity. Failing to recognise this opportunity led the authors of those previous work to impose additional requirements onto their systems (e.g., node synchronisation, tightly controlled transmission timing, ad-hoc ranging protocols) or abandon time-based ranging techniques in favour of less accurate power-based ranging.

In the general scenario depicted in Fig. 1(a) reference transmitters and receivers are regarded as independent entities. For several real-world applications, particularly those involving WiFi deployments and Wireless Sensor Networks (WSN), it makes sense to consider a particularisation of this model with a single set of "anchor" nodes in (known) fixed positions, each anchor serving both as (reference) transmitter and receiver. In other words, reference transmitters and receivers are 1:1 coupled, as depicted in Fig. 1(b). Motivated by the practical relevance of this scenario, and by the advantage of a certain notational simplification in this case, hereafter we focus the presentation of the proposed method and of the numerical results to the particular scenario of Fig. 1(b), with the understanding that all proposed algorithms can be generalised straightforwardly to the more general case of independent transmitters depicted in Fig. 1(a).

In this work we formalise the tracing/localisation problem within the system model outlined above and present a possible resolution strategy. Along the way, we provide different variants of Least Squares (LS) estimators based on Time of Arrival (TOA) and Time-Difference of Arrival (TDOA). As a by-product of this study, we prove the equivalence of the TOA and TDOA instances for the problem at hand — a result that strengthens and generalises previous results about TOA and TDOA "equivalence". Numerical results from Monte Carlo simulations are provided to explore the impact of various system-level aspects and parameters. For the special case of null blind velocity (localisation problem), the proposed method is compared against an alternative approach based on Differential Time-Difference of Arrival (DTDOA) that was published in a previous work [7]. Finally, results are validated on experimental data from a real-world WiFi testbed.

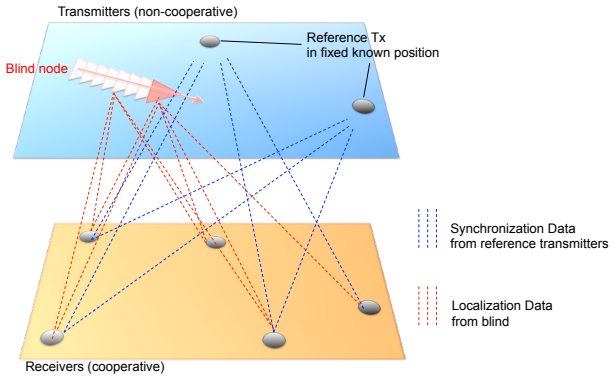

(a) General scenario with independent reference transmitters (non-cooperative) and receivers (cooperative).

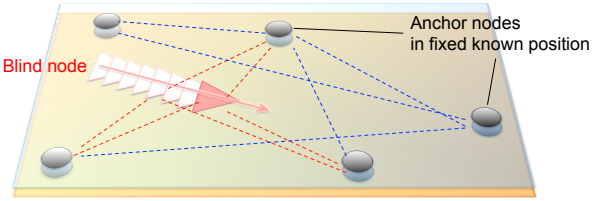

(b) Particularized scenario: each anchor node serves both as receiver and reference transmitter.

Figure 1. Reference scenario.

2 System Model

The reference scenario is depicted in Fig. 1(b). Consider a system with $N+1$ nodes indexed with $n = 0, \ldots, N$. Index $n = 0$ is reserved for the (moving) blind node, whose trajectory parameters we wish to estimate, whereas the remaining N (anchor) nodes are placed in fixed known positions. We assume a minimum of five anchors, i.e. $N \geq 5$. During the observation interval, the blind node transmits M (data) packets, while the generic anchor n transmits B_n (beacon) packets. We shall indicate by $G \stackrel{\text{def}}{=} \sum_{n=1}^{N} B_n$ the total number of beacon packets transmitted by all anchors. Each packet may be overheard and timestamped by any other anchor node (except the sender, in case of beacon packets) and all the collected measurements are sent to a central computation entity.

In an ideal system with zero packet loss every packet is timestamped by all potential receivers, resulting in a complete dataset of $MN+G(N-1)$ measurements. However, in real systems occasional packet loss cannot be avoided (e.g., due to interference or collisions) and therefore must be taken into account in the system model. To illustrate, we sketch graphically in Fig. 2(a) an example of lossy dataset, where each transmitted packet (top row) is received by only a subset of possible receivers. Since the transmission time of a generic packet m is unknown, the individual TOA measurement at a single anchor does not carry any useful information about the receiver position relative to the transmitter. However, if we consider the collection of TOA measurements for the same packet at two or more anchor nodes, they *collectively*

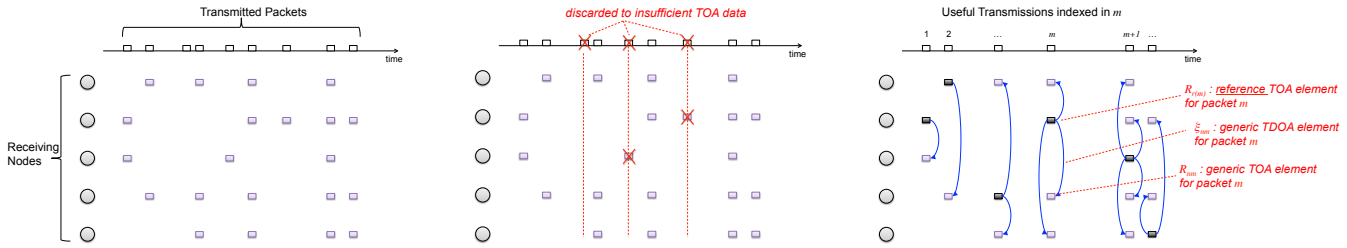

(a) Initial lossy dataset

(b) Data pre-filtering: packets received by a single node are discarded.

(c) For each useful transmission m, a single pivot anchor $\overline{n}_m$ is randomly selected.

Figure 2. Graphical representation of dataset pre-processing.

carry information about the relative node positions. In other words, a generic packet transmitted at an unknown time produces useful information for the localisation problem only if it is received (and timestamped) by at least two anchors. For this reason, we preliminarily discard the reception timestamps associated to packets that were received by a single anchor. The resulting filtered dataset, sketched in Fig. 2(b), represents the input for the proposed algorithm.

The following notation is introduced:

- $\mathcal{A} \stackrel{\text{def}}{=} \{1, \dots, N\}$ is the set of all anchor nodes.
- $\mathcal{A}_m \subseteq \mathcal{A}$ is the subset of anchor nodes that have successfully received and timestamped packet m.
- $N_m \stackrel{\text{def}}{=} |\mathcal{A}_m|$ is the number of receiving anchors for packet m. The pre-filtering stage guarantees $N_m \geq 2$.
- $i(m) \in \{0, \dots, N\}$ denotes the transmitting node index for the generic mth packet. As the source node cannot hear its own packet, $i(m) \notin \mathcal{A}_m$.
- T is the duration of the observation window, i.e., the maximum age of the data used for the estimation.
- $t_m \in [0, T]$ is the unknown transmission time of packet m by node $i(m)$.
- $\overline{n}_m \in \mathcal{A}_m$ is the "reference anchor" for packet m, chosen arbitrarily among the elements of $\mathcal{A}_m$.
- R_{nm} is the reception timestamp of the mth packet at the receiving node n as measured by its local clock.
- e_{nm} is a random error term (measurement noise) affecting the reception timestamp R_{nm}.
- θ_n is the (unknown) clock offset term for node n.
- γ_n is the (unknown) clock skew factor for node n, i.e., the relative difference between the actual and nominal clock frequency.
- $\boldsymbol{q}_n \stackrel{\text{def}}{=} [x_n, y_n, z_n]$ is the 3D position of generic anchor node $n = 1, \dots, N$ in the reference system.
- $\boldsymbol{p} \stackrel{\text{def}}{=} [p_x, p_y, p_z]$ is the actual position of the blind node at the end of the observation window $t = T$.
- $\boldsymbol{v} \stackrel{\text{def}}{=} [v_x, v_y, v_z]$ the velocity vector of the blind node in the reference 3D coordinate system.
- $\boldsymbol{p}(t) = \boldsymbol{p} - \boldsymbol{v}(T - t)$ is the instantaneous position of the blind node at the generic time $t \in [0, T]$.
- $d_{k,n} \stackrel{\text{def}}{=} \|\boldsymbol{p}_k - \boldsymbol{q}_n\| = d_{n,k}$ is the Euclidean distance between nodes k and n.

For ease of notation we stack the variables θ_n and γ_n, $n = 1, \dots, N$ into the vectors $\boldsymbol{\theta}$ and $\boldsymbol{\gamma}$, respectively.

We assume that the measurements errors e_{nm} are i.i.d. with zero-mean and variance σ_e^2. These assumptions are reasonable in practical deployments with homogeneous commercial-off-the-shelf (COTS) devices, where the timing accuracy is typically limited by the ADC rate and/or clock resolution. Furthermore, if the error distribution can be assumed gaussian, then the Least Squares (LS) estimators developed throughout the paper represent the optimal Maximum Likelihood (ML) estimators.

In addition to (random) measurement errors, we assume that the timing measurements of the generic node n are affected by two systematic error terms: a temporal offset θ_n and a (relative) frequency offset γ_n. In other words, the various nodes clocks are free to run without any synchronisation nor tuning mechanism. We consider a simplified scenario where signal propagation occurs through direct Line-of-Sight (LOS) path between any pair of nodes. The LOS assumption is very common in time-based localisation studies, and most previous work are based on full LOS models, e.g. [1], [2], [3], [4], [6], [8], [9], [10], [11], [12], [13], [14], [15], [16], [17], [18], [19].

The 3D positions of all anchor nodes are known exactly without error. We assume the blind node position to be constrained on the horizontal plane (hence $v_z = 0$) at known height p_z, and the problem is to determine the horizontal components $[p_x, p_y, v_x, v_y]$. With the above notation, the reception timestamp measured at anchor n for the mth packet sent by another anchor $i(m) \neq n$ writes as (**anchor-to-anchor equation**):

$$(1 + \gamma_n)\, R_{nm} = t_m + \frac{d_{n,i(m)}}{c} + \theta_n + e_{nm} \qquad (1)$$

where $d_{n,i(m)} \stackrel{\text{def}}{=} \|\boldsymbol{p}_{i(m)} - \boldsymbol{q}_n\|$ denotes the (known) distance between the transmitting and receiving anchors, and c the speed of light. If, instead, the mth packet is transmitted by the blind node, the reception timestamp at anchor n writes as (**blind-to-anchor equation**):

$$(1 + \gamma_n)\, R_{nm} = t_m + \frac{1}{c}\|\boldsymbol{p} - \boldsymbol{v}(T - t_m) - \boldsymbol{q}_n\| + \theta_n + e_{nm}. \quad (2)$$

The overall resolution method relies on the model equations (1) and (2) and it is sketched in Fig. 2. We devise a two-stage approach, where synchronisation and localisation (or tracing) are performed by two distinct routines. First, clock error terms $\hat{\boldsymbol{\theta}}, \hat{\boldsymbol{\gamma}}$ are estimated

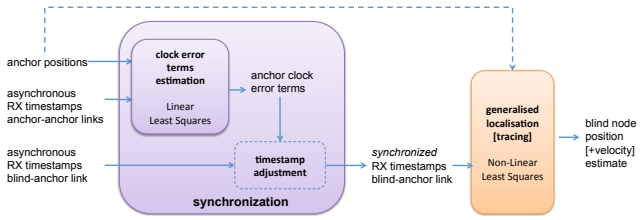

Figure 3. Workflow of the proposed method.

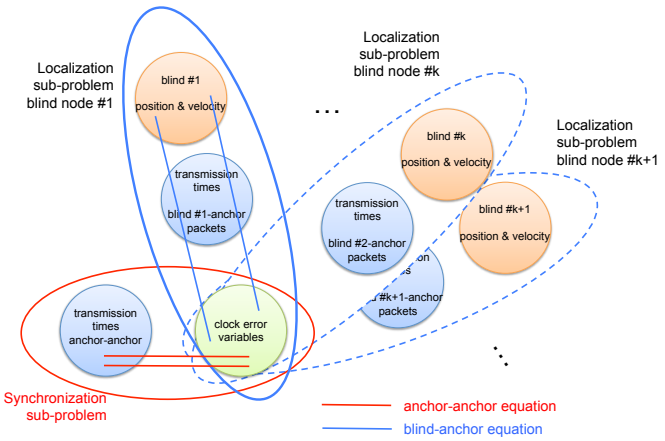

Figure 4. Graphical representation of the search space.

from anchor-anchor measurements with the method presented later in Sec. 3, and used to correct the blind-anchor timestamps. In the second stage, the adjusted blind-anchor timestamps are used to determine $\boldsymbol{p}$ and $\boldsymbol{v}$ with the algorithms developed later in Sec. 4.

Hereafter we motivate the choice of a two-stages approach. In fact, it is possible in principle to join the estimation of clock error parameters and trajectory parameters into a single larger estimation instance — an approach followed e.g. by [8], [9] for a different scenario. While this approach might seem more compact, it would come at the cost of higher complexity due to the larger dimensionality of the search space, with no clear benefit in terms of final accuracy. To elaborate, we sketch in Fig. 4 an abstract representation of the overall problem structure. The red and blue lines represent, respectively, anchor-to-anchor equations of type (1) and blind-to-anchor equations of type (2). Notably the variable sub-spaces spanned by the two sets of measurements intersect only at the sub-space of clock error variables. Since the latter can be fully determined by anchor-to-anchor measurements, that are abundant in practice, there is no benefit in merging together the two sub-sets of measurements in a single joint estimation instance of much larger dimensionality. The advantage of the split approach is reinforced by the fact that the synchronisation sub-problem defined in Sec. 3 (red oval in Fig. 4) is linear, hence can be solved directly in closed-form. Moreover, the advantage of the split approach is amplified when multiple blind nodes are to be traced in parallel. Since the blind nodes are non-cooperating, no blind-to-blind measurement is available to tie together the position/velocity variables of different nodes, and therefore the localisation sub-problem for can be naturally decoupled for different sources, letting each blind node being traced independently from the others. In other words, the splitting between localisation and synchronisation sub-problems avoids the unnecessary duplication of clock error estimation.

3 Estimation of Clock Error Terms (Data Synchronisation)

For the first stage, we follow a procedure similar in spirit to the synchronisation method adopted in [10] for a very different system model (therein knowledge of transmission times and two-way ranging between node pairs were considered).

We start noting that the generic anchor-to-anchor equation (1) is linear into the unknown variables θ_n, γ_n ($n = 1, \dots, N$) and t_m ($m = 1, \dots, G$). Therefore the estimation problem can be cast into a linear LS problem, for which a closed form solution can be computed directly. However, careful analysis reveals that the problem is underdetermined, i.e., it does not have a unique solution (see discussion in [10, Sec. VI]). To remove the ambiguity, it is sufficient to pick one anchor to serve as clock reference: without loss of generality we pick the first anchor with $n = 1$ as reference, and set $\hat{\theta}_1 = 0$ and $\hat{\gamma}_1 = 0$ as fixed parameters. It is obvious that setting $\hat{\theta}_1 = 0$ is inconsequential for the estimation process, since we have one degree of freedom in setting the origin of the time axis. As for the constraint $\hat{\gamma}_1 = 0$, we will show later that the impact on the final estimate is absolutely negligible.

With these settings we are left with $2(N-1)$ clock error terms plus G unknown transmission times to estimate. For a more compact matrix notation we define the variable vector $\boldsymbol{y} \stackrel{\text{def}}{=} [\theta_2, \dots, \theta_N, \gamma_2, \dots, \gamma_N, t_1, \dots, t_G]^T$ of length $2(N-1)+G$. In order to represent the available measurements in matrix form, we map all possible GN measurements (for G packets at N anchors) to a single index $k = (m-1)N + n$, with $m = 1, \dots, G$ and $n = 1, \dots, N$. Denote by $\boldsymbol{b}$ the vector of length GN with elements defined by:

$$b_k \stackrel{\text{def}}{=} \begin{cases} d_{n,i(m)}/c - R_{nm} & \text{if } n \in \mathcal{A}_m \\ 0 & \text{otherwise} \end{cases}$$

with $k = (m-1)N + n$. Denote by $\boldsymbol{H}$ the matrix of size $GN \times 2(N-1) + G$ with elements h_{kj} defined as

$$h_{kj} \stackrel{\text{def}}{=} \begin{cases} -1 & \text{if } j = n,\ n \geq 2,\ n \in \mathcal{A}_m \\ R_{nm} & \text{if } j = N + n - 2,\ n \geq 2,\ n \in \mathcal{A}_m \\ -1 & \text{if } j = 2N - 2 + m \text{ and } n \in \mathcal{A}_m \\ 0 & \text{otherwise} \end{cases}$$

wherein again $k = (m-1)N + n$. With the above notation, and considering that all timestamp errors are assumed i.i.d., the linear LS estimate derived from the model

This article has been accepted for publication in a future issue of this journal, but has not been fully edited. Content may change prior to final publication. Citation information: DOI 10.1109/TMC.2018.2792443, IEEE Transactions on Mobile Computing

equations (1) writes as:

$$\hat{\boldsymbol{y}} = \arg\min_{\boldsymbol{y}} (\boldsymbol{H}\boldsymbol{y} - \boldsymbol{b})^T (\boldsymbol{H}\boldsymbol{y} - \boldsymbol{b}) = \boldsymbol{H}^+ \boldsymbol{b} \tag{3}$$

wherein $\boldsymbol{H}^+$ is the Moore-Penrose pseudo-inverse of $\boldsymbol{H}$.

After estimating the clock error terms $\hat{\theta}_n, \hat{\gamma}_n$ from anchor-to-anchor measurements, all reception timestamps for blind-to-anchor packets can be corrected. The generic adjusted timestamp will be denoted by

$$R'_{nm} \stackrel{\text{def}}{=} (1 + \hat{\gamma}_n) \cdot R_{nm} - \hat{\theta}_n. \tag{4}$$

This procedure is equivalent to align all anchor clocks to the clock of the reference anchor, leaving only an unknown offset ("inherited" by the reference anchor) between the common clock frequency, equal for all anchors after timestamp adjustment, and the nominal frequency. We will show later in Sec. 4.5 that the effect of such small *common* frequency offset is absolutely negligible in practice, therefore we will disregard it in the analysis.

4 Position and Velocity Estimation

4.1 Preliminaries

Replacing the raw timestamps with the adjusted timestamps (4), the blind-to-anchor equation (2) after data synchronisation rewrites as:

$$R'_{nm} = t_m + \frac{1}{c}\|\boldsymbol{p} - \boldsymbol{v} \cdot (T - t_m) - \boldsymbol{q}_n\| + e_{nm}. \tag{5}$$

Based on this model equation, we can cast the tracing problem into a Non-linear LS form. However, before proceeding further we introduce a small but important simplification in the basic model equation (5): we approximate the (unknown) packet transmission time appearing in the distance term by the (known) arrival time at some reference anchor. For every packet m, we pick arbitrarily one of the receiving anchors $\overline{n}_m \in \mathcal{A}_m$ to serve as reference. We shall denote by $\overline{R'_m} \stackrel{\text{def}}{=} R'_{nm}|_{n=\overline{n}_m}$ the (adjusted) reception timestamp associated to the reference anchor $\overline{n}_m$. After replacing t_m with $\overline{R'_m}$ in the distance term, eq. (5) rewrites as:

$$R'_{nm} \cong t_m + \frac{1}{c}\|\boldsymbol{p} - \boldsymbol{v} \cdot (T - \overline{R'_m}) - \boldsymbol{q}_n\| + e_{nm}. \tag{6}$$

The transmission time t_m now appears only as an additive term. The error on the final position estimate introduced by approximating $t_m \approx \overline{R'_m}$ into the distance term is in the order of $\frac{|v|}{c}$ times the distance between the blind node and the reference anchor, and can be safely neglected in practical applications. For example, with blind node speed of $|v| = 10$ m/s at a distance of 300 meters from the reference anchor, the approximation error is in the order of 10^{-5} meters.

In order to reduce numerical errors, we recenter the timestamp data for each packet m around the reference time $\overline{R'_m}$, and rescale all terms by the speed of light c. To this aim we define the new terms

$$\tilde{R}_{nm} \stackrel{\text{def}}{=} \left(R'_{nm} - \overline{R'_m}\right) \cdot c \tag{7a}$$

$$\tilde{t}_m \stackrel{\text{def}}{=} \left(t_m - \overline{R'_m}\right) \cdot c \tag{7b}$$

$$\tilde{e}_{nm} \stackrel{\text{def}}{=} e_{nm} \cdot c. \tag{7c}$$

With these definitions the basic equation (6) rewrites as:

$$\tilde{R}_{nm} = \tilde{t}_m + \|\boldsymbol{p} - \boldsymbol{v} \cdot (T - \overline{R'_m}) - \boldsymbol{q}_n\| + \tilde{e}_{nm}. \tag{8}$$

Note the difference between the terms $\tilde{R}_{nm}$ (re-centered and re-scaled by c) and $\overline{R'_m}$ used, respectively, outside and inside the distance term. We remark that both $\tilde{R}_{nm}$ and $\overline{R'_m}$ are computed directly from the input data.

For the sake of simpler notation we gather all the variables of interest into the vector $\boldsymbol{z} \stackrel{\text{def}}{=} [\boldsymbol{p}, \boldsymbol{v}] = [p_x, p_y, v_x, v_y]$ and all nuisance variables into the vector $\boldsymbol{t} \stackrel{\text{def}}{=} \left[\tilde{t}_1, \ldots, \tilde{t}_M\right]$, and denote the non-linear terms by

$$d_{nm}(\boldsymbol{z}) \stackrel{\text{def}}{=} \|\boldsymbol{p} - \boldsymbol{v} \cdot (T - \overline{R'_m}) - \boldsymbol{q}_n\|. \tag{9}$$

With these positions the basic equation (8) rewrites as

$$\tilde{R}_{nm} = \tilde{t}_m + d_{nm}(\boldsymbol{z}) + \tilde{e}_{nm}. \tag{10}$$

If the error terms $\tilde{e}_{nm}$ are i.i.d. and gaussian, the negative log-likelihood function is given by

$$\ell(\boldsymbol{z}, \boldsymbol{t}) = \frac{1}{2} \sum_{m=1}^{M} \sum_{n \in \mathcal{A}_m} \left(\tilde{t}_m + d_{nm}(\boldsymbol{z}) - \tilde{R}_{nm}\right)^2. \tag{11}$$

4.2 TOA formulation

In the first TOA variant the (unknown) transmission times $\boldsymbol{t}$ are treated as nuisance variables to be estimated jointly with the variables of interest $\boldsymbol{z}$. The minimisation of the negative log-likelihood function (11) leads to the following Non-linear Least Squares (NLS) form:

$$\begin{aligned}
\hat{\boldsymbol{z}}, \hat{\boldsymbol{t}} &= \arg\min_{\boldsymbol{z}, \boldsymbol{t}} \sum_{m=1}^{M} \sum_{n \in \mathcal{A}_m} \ell(\boldsymbol{z}, \boldsymbol{t}) \\
&= \arg\min_{\boldsymbol{z}, \boldsymbol{t}} \sum_{m=1}^{M} \sum_{n \in \mathcal{A}_m} \left(\tilde{t}_m + d_{nm}(\boldsymbol{z}) - \tilde{R}_{nm}\right)^2 \\
&= \arg\min_{\boldsymbol{p}, \boldsymbol{v}, \boldsymbol{t}} \sum_{m=1}^{M} \sum_{n \in \mathcal{A}_m} \left(\tilde{t}_m + \|\boldsymbol{p} - \boldsymbol{v} \cdot (T - \overline{R'_m}) - \boldsymbol{q}_n\| - \tilde{R}_{nm}\right)^2.
\end{aligned} \tag{12}$$

The NLS estimator (12) corresponds to the Maximum Likelihood (ML) estimator if the errors are i.i.d. and gaussian, and in this case the solution is optimal in the ML sense. If errors are i.i.d. unbiased but not gaussian[2], the solution delivered by the NLS method is not optimal *relatively to the achievable bound*, but in absolute terms its accuracy remains pretty similar to that of the gaussian case (ref. Fig. 9 and discussion thereafter).

2. This is often the case in practical scenarios deploying homogeneous COTS devices, since the reception timestamp reported by commercial receivers is typically obtained by the first sample of the detected preamble. In this case, timestamp resolution is limited by the ADC sampling rate of the radio front-end a more limiting factor than the theoretically achievable bound (see e.g. [20]).

This article has been accepted for publication in a future issue of this journal, but has not been fully edited. Content may change prior to final publication. Citation information: DOI 10.1109/TMC.2018.2792443, IEEE Transactions on Mobile Computing

4.3 TDOA formulation

In the alternative Time-Difference of Arrival (TDOA) variant the (unknown) transmission time variable $\tilde{t}_m$ is eliminated by taking the difference of arrival times at different anchors. Subtraction introduces correlation between the residuals, hence the need to consider a non-diagonal covariance matrix. For a generic packet m sent by the blind node, consider the reference anchor $\overline{n}_m$ and another receiving anchor $n \neq \overline{n}_m$, and denote the difference between their respective TOA residuals by:

$$\xi_{nm} \stackrel{\text{def}}{=} \tilde{e}_{nm} - \tilde{e}_{\overline{n}_m m} = \tilde{R}_{nm} - d_{nm}(\boldsymbol{z}) + \overline{d}_m(\boldsymbol{z}) \qquad (13)$$

wherein $\overline{d}_m(\boldsymbol{z}) \stackrel{\text{def}}{=} d_{nm}(\boldsymbol{z})|_{n=\overline{n}_m}$ is the distance term associated to the reference anchor. Recall that by definition the re-centered timestamp of the reference anchor is zero, i.e., $\tilde{R}_{nm}|_{n=\overline{n}_m} \equiv 0$. The term ξ_{nm} represents the TDOA residual for packet m associated to the pair of receiving anchors n and $\overline{n}_m$. For the sake of notational simplicity, we stack into the vector $\boldsymbol{\xi}_m \stackrel{\text{def}}{=} \{\xi_{nm},\, n \in \mathcal{A}_m \backslash \overline{n}_m\}$ all TDOA residuals for packet m. Due to the presence of a common term, the components of vector $\boldsymbol{\xi}_m$ are not independent, and therefore the (generalized) LS form must take into account the non-diagonal covariance matrix of $\boldsymbol{\xi}_m$, denoted by $\boldsymbol{\Sigma}_m$. For the particular case at hand, $\boldsymbol{\Sigma}_m$ has a particularly simple structure, independent of the choice of the reference anchor, with all diagonal elements equal to '2' and all off-diagonal elements equal to '1'. Hence can be written as the sum $\boldsymbol{\Sigma}_m = \boldsymbol{I} + \boldsymbol{O}_{[N_m-1]}$, where $\boldsymbol{I}$ is the identity matrix and $\boldsymbol{O}_k$ denotes a square $k \times k$ matrix with all unitary elements. By the Sherman-Morrison theorem [21] the inverse develops as:

$$\boldsymbol{\Sigma}_m^{-1} \stackrel{\text{def}}{=} \left(\boldsymbol{I} + \boldsymbol{O}_{[N_m-1]}\right)^{-1} = \boldsymbol{I} - \frac{1}{N_m}\boldsymbol{O}_{[N_m-1]}.$$

Thanks to the simple structure of $\boldsymbol{\Sigma}_m^{-1}$, the TDOA estimator can be developed into the following simple form (**TDOA formulation**):

$$\begin{aligned}\hat{\boldsymbol{z}} &= \arg\min_{\boldsymbol{z}} \sum_{m=1}^{M} \boldsymbol{\xi}_m^T \boldsymbol{\Sigma}_m^{-1} \boldsymbol{\xi}_m \\ &= \arg\min_{\boldsymbol{z}} \sum_{m=1}^{M} \left(\sum_{\substack{n\in\mathcal{A}_m \\ n\neq\overline{n}_m}} \xi_{nm}^2 - \frac{1}{N_m} \left(\sum_{\substack{n\in\mathcal{A}_m \\ n\neq\overline{n}_m}} \xi_{nm} \right)^2 \right).\end{aligned} \qquad (14)$$

Note that the search space of (14) has lower dimensionality than (12) since the nuisance variables $\boldsymbol{t}$ have been eliminated. As for the variables of interest $\boldsymbol{z}$, we will show below that TOA and TDOA estimators represented respectively by (12) and (14) *lead exactly to the same solution* $\hat{\boldsymbol{z}}$ when instantiated with the same input data.

4.4 S-TOA formulation

Starting from the TOA formulation (12) it is possible to derive an alternative formulation, with the same (lower) dimensionality of the TDOA form (14), but without the need of introducing pairwise timestamp differences. We will refer to this new formulation by the term "S-TOA" for "shrunk TOA". For ease of notation let

$$f_{nm}(\boldsymbol{z}) \stackrel{\text{def}}{=} d_{nm}(\boldsymbol{z}) - \tilde{R}_{nm} = \|\boldsymbol{p} - \boldsymbol{v}\cdot(T - \overline{R'_m}) - \boldsymbol{q}_n\| - \tilde{R}_{nm}.$$

Recall that the solution $\hat{\boldsymbol{z}}$ to the unconstrained minimisation (12) must satisfy the zero-gradient condition:

$$\begin{aligned}&\frac{\partial}{\partial \tilde{t}_i} \sum_{m=1}^{M} \sum_{n\in\mathcal{A}_m} \left(\tilde{t}_m + f_{nm}(\boldsymbol{z})\right)^2 = 0, \quad i = 1,\ldots,M \\ &\Rightarrow \tilde{t}_m = -\frac{1}{N_m} \sum_{n\in\mathcal{A}_m} f_{nm}(\boldsymbol{z}), \qquad m = 1,\ldots,M.\end{aligned} \qquad (15)$$

hence replacing $\tilde{t}_m$ in the objective function (12) with the last term of (15) does not change the solution in the space of $\boldsymbol{z}$. Doing so, after some trivial passages (12) rewrites:

$$\begin{aligned}\hat{\boldsymbol{z}} &= \arg\min_{\boldsymbol{z}} \sum_{m=1}^{M} \sum_{n\in\mathcal{A}_m} \left(f_{nm}(\boldsymbol{z}) - \frac{1}{N_m} \sum_{n\in\mathcal{A}_m} f_{nm}(\boldsymbol{z}) \right)^2 \\ &= \arg\min_{\boldsymbol{z}} \sum_{m=1}^{M} \left(\sum_{n\in\mathcal{A}_m} f_{nm}^2(\boldsymbol{z}) - \frac{1}{N_m} \left(\sum_{n\in\mathcal{A}_m} f_{nm}(\boldsymbol{z}) \right)^2 \right).\end{aligned} \qquad (16)$$

Note that we have effectively eliminated the variables $\tilde{t}_m$, reducing the dimensionality of the search space.

4.5 Insensitivity to a common frequency shift

In this section we prove that the presence of a small *common* offset from the nominal clock frequency affecting all input timestamps is inconsequential for the position and velocity estimation, and therefore can be neglected. Recall from Sec. 3 that a common frequency offset is "inherited" by the clock of the anchor selected to serve as clock reference. We derive the proof for the S-TOA formulation (16), but since the solution of TOA and TDOA is exactly the same as S-TOA, the proof is valid for all these formulations.

Denote by $\gamma << 1$ the (unknown) relative frequency offset term. To model a common frequency offset, all measurement data should be rescaled by $(1+\gamma)$, i.e., each term $\tilde{R}_{nm}$ should be replaced by $(1+\gamma)\tilde{R}_{nm}$. Accordingly, the term $f_{nm}(\boldsymbol{z}) \stackrel{\text{def}}{=} \|\boldsymbol{p}-\boldsymbol{v}\cdot(T-\overline{R'_m})-\boldsymbol{q}_n\|-\tilde{R}_{nm}$ appearing in (16) should be replaced by

$$\begin{aligned}f'_{nm}(\boldsymbol{z}) &\stackrel{\text{def}}{=} \|\boldsymbol{p} - \boldsymbol{v}\cdot(T - \overline{R'_m}) - \boldsymbol{q}_n\| - (1+\gamma)\tilde{R}_{nm} \\ &= (1+\gamma)\left(\|\boldsymbol{p}' - \boldsymbol{v}'\cdot(T - \overline{R'_m}) - \boldsymbol{q}'_n\| - \tilde{R}_{nm}\right)\end{aligned}$$

wherein $\boldsymbol{p}' \stackrel{\text{def}}{=} \frac{1}{1+\gamma}\boldsymbol{p}$, $\boldsymbol{v}' \stackrel{\text{def}}{=} \frac{1}{1+\gamma}\boldsymbol{v}$ and $\boldsymbol{q}'_n \stackrel{\text{def}}{=} \frac{1}{1+\gamma}\boldsymbol{q}_n$ denote the spatial vectors in a reference system rescaled by $\frac{1}{1+\gamma}$. Since the $\arg\min(\cdot)$ function is insensitive to a multiplicative rescaling it holds that $\arg\min \sum_{n,m}(1+\gamma)x_{nm} = \arg\min(1+\gamma)\sum_{n,m} x_{nm} = \arg\min \sum_{n,m} x_{nm}$, therefore the outer factor $(1+\gamma)$ is irrelevant in the minimisation (16) and the only residual effect is the whole geometry rescaling. The relative error caused by such rescaling is in the order of $|\gamma|$, since $\gamma << 1 \Rightarrow \frac{1}{1+\gamma} \approx 1-\gamma$. For example, for a COTS device

This article has been accepted for publication in a future issue of this journal, but has not been fully edited. Content may change prior to final publication. Citation information: DOI 10.1109/TMC.2018.2792443, IEEE Transactions on Mobile Computing

with frequency tolerance $|\gamma| \leq 10$ ppm and a network of $d_{max} = 300$ meters the error due to geometrical rescaling remains below 3 mm, hence negligible in practice.

5 Discussion

5.1 On the different forms of "equivalence" between non-linear estimators

Consider two generic estimators in the form

$$\hat{\boldsymbol{z}}_1 = \arg\min_{\boldsymbol{z}\in\mathcal{X}} \phi_1(\boldsymbol{z}) \quad \text{and} \quad \hat{\boldsymbol{z}}_2 = \arg\min_{\boldsymbol{z}\in\mathcal{X}} \phi_2(\boldsymbol{z})$$

with non-linear but differentiable objective functions $\phi_i(\boldsymbol{z})$ $(i = 1, 2)$ to be solved numerically by some gradient-based method. We distinguish the following types of relationship between the two estimators above:

(I) **Equality** if $\hat{\boldsymbol{z}}_1 = \hat{\boldsymbol{z}}_2 \Leftarrow \phi_1(\boldsymbol{z}) = \phi_2(\boldsymbol{z})$, $\forall \boldsymbol{z} \in \mathcal{X}$.
(II) **Strong Equivalence** if $\hat{\boldsymbol{z}}_1 = \hat{\boldsymbol{z}}_2$ but $\phi_1(\boldsymbol{z}) \neq \phi_2(\boldsymbol{z})$.
(III) **Weak Equivalence** if $\hat{\boldsymbol{z}}_1 \neq \hat{\boldsymbol{z}}_2$ but $E\{\hat{\boldsymbol{z}}_1\} = E\{\hat{\boldsymbol{z}}_2\}$ and $VAR\{\hat{\boldsymbol{z}}_1\} = VAR\{\hat{\boldsymbol{z}}_2\}$.

Two "equal" estimators in the sense of definition (I) have the same objective function (hence same gradient) across the entire search space $\mathcal{X}$. Consequently, the numerical procedure will follow the very same numeric path and eventually converge exactly to the same solution (or not converge at all). In other words, the two forms are merely different analytical representations of the very same estimator.

Two "strongly equivalent" estimators in the sense of definition (II) have different objective functions but the same global minimum. They should theoretically lead to the very same final solution, notwithstanding the usual risks of numerical procedures (local minima, divergence). However, even in the desirable case that the adopted resolution algorithm is capable of converging to the global optimum, the search path will be in general different for the two forms. It practice, we may find that one or the other form yields systematically better convergence behaviour (e.g., converges with higher probability to the global optimum in less iterations) and therefore should be preferred. In other words, "strong equivalence" of two analytical forms does not mean that their performances are undistinguishable in practice.

Two "weakly equivalent" estimators in the sense of definition (III) will lead in general to different solutions. However, the two solutions have the same accuracy, i.e., same variance of final estimation error. If we denote by $\boldsymbol{z}^*$ the true value of the variable(s) we wish to estimate, it can be easily seen that the definition of weak equivalence implies that $E\left\{(\hat{\boldsymbol{z}}_1 - \boldsymbol{z}^*)^2\right\} = E\left\{(\hat{\boldsymbol{z}}_2 - \boldsymbol{z}^*)^2\right\}$.

5.2 Equality of TDOA and S-TOA

From the definition (13) it holds that $\xi_{mn} = f_{mn}(\boldsymbol{z}) - \overline{d}_m(\boldsymbol{z})$. Comparing (16) to (14), it is evident a strong similarity between the objective functions. In fact, S-TOA and TDOA can be written in the common format:

$$\hat{\boldsymbol{z}} = \arg\min_{\boldsymbol{z}} \sum_{m=1}^{M} v\left(g_{1m}, \ldots, g_{Nm}\right)$$

with $v\left(x_1, \ldots, x_N\right) \stackrel{\text{def}}{=} \sum_{n=1}^{N} x_n^2 - \frac{1}{N}\left(\sum_{n=1}^{N} x_n\right)^2$ and the terms g_{nm} defined[3] as:

$$g_{nm} \stackrel{\text{def}}{=} \begin{cases} f_{nm}(\boldsymbol{z}) - \overline{d}_m(\boldsymbol{z}) & \text{for TDOA,} \\ f_{nm}(\boldsymbol{z}) & \text{for S-TOA.} \end{cases} \tag{17}$$

The term $v\left(x_1, \ldots, x_N\right)$ represents the sum of squared deviations from the mean for the set $\{x_n,\ n = 1, \ldots, N\}$, and rescaling by $\frac{1}{N-1}$ would lead to the canonical expression for the sample variance. Likewise the sample variance, $v(\cdot)$ is invariant to translation by a common term μ, formally:

$$v\left(x_1, x_2, \ldots, x_N\right) = v\left(x_1 - \mu, x_2 - \mu, \ldots, x_N - \mu\right),\ \forall \mu$$

as can be easily verified with a few simple algebraic passages. From (17) we immediately recognise that this is indeed the case when comparing TDOA and S-TOA, with $\overline{d}_m(\boldsymbol{z})$ in (17) playing the role of the common shift μ. Therefore, we conclude that *TDOA and S-TOA yield the same value of the objective function for any generic point $\boldsymbol{z}$ of the search space*. In other words, they are perfectly "equal" in the sense of definition (I), i.e., *TDOA and S-TOA are merely two ways of expressing the same estimator*, and for this reason hereafter we will use the labels TDOA and S-TOA interchangeably.

5.3 Strong equivalence of TOA and TDOA/S-TOA

By construction (ref. Sec. 4.4) S-TOA leads to the same solution of TOA in the space of the variable of interest $\boldsymbol{z}$. In other words, they are "strongly equivalent" in the sense of definition (II). Together with equality of S-TOA and TDOA, this means that TOA and TDOA are also "strongly equivalent", i.e., their theoretical solution is exactly the same. This is a new result that *strengthens* and *generalizes* previous results comparing TOA and TDOA solutions. In fact, previous work dealing with static node localisation had proved only "weak equivalence", based on the comparison of the respective Cramer-Rao bounds (see e.g. [22] and references therein). The only explicit "strong equivalence" demonstration that we found in the literature appears in [23, Theorem 2], limited to linearised (approximated) versions of the TOA and TDOA estimator and for the special case of a static node. We remark that the our proof applies to any generic set of non-linear functions $f_{nm}(\boldsymbol{z})$ in the generic vector of variables $\boldsymbol{z}$. As such, it applies to *any arbitrary parametric trajectory*, including but not limited to the linear motion that is the focus of the present work, and represents a generalisation of the result in [23, Theorem 2].

5.4 Particularisation to a static emitter (localisation)

In the previous section we have developed estimators for the "tracing" problem (following the definition in [1]) where the unknown velocity $\boldsymbol{v}$ of a linearly moving

3. Since $\xi_{nm}|_{n=\overline{n}_m} = 0$ the inner sum in (14) can be extended to the whole set $\mathcal{A}_m$, i.e. $\sum_{n\in\mathcal{A}_m,\ n\neq\overline{n}_m} \xi_{nm} = \sum_{n\in\mathcal{A}_m} \xi_{nm}$.

node must be estimated in addition to the final position $\boldsymbol{p}$. Since all estimators ultimately lead to exactly the same solution, we shall refer to them collectively as "TOA/TDOA" estimators hereafter. In the particular case that the blind node is known to be static, the tracing problem reduces to the classic *static localisation* problem. We have two different options to address the static localisation problem with our estimators:

- **Dynamic TOA/TDOA**. With this approach we use any of the estimators derived above where velocity $\boldsymbol{v}$ appears as an unknown variable. The solution will in general deliver a small but non-zero velocity estimate $\hat{\boldsymbol{v}}$ (the estimator will "interpret" part of the measurement noise as node movement). The mid-point of the estimated trajectory $\hat{\boldsymbol{p}} - \frac{1}{2}\hat{\boldsymbol{v}}T$ is then selected as the estimate of the (fixed) node position.
- **Static TOA/TDOA**. With this approach the information about the node being static is encoded *ex ante* into the estimator. Any of the estimators derived above can be used, but their formulation is particularised by setting $\boldsymbol{v} = 0$ into the function $d_{mn}(\cdot)$ leaving the position $\hat{\boldsymbol{p}}$ as the only variable of interest to be determined. In other words, (9) is replaced by $d_{nm}(\boldsymbol{z}) \stackrel{\text{def}}{=} \|\boldsymbol{p} - \boldsymbol{q}_n\|$.

Alternatively, we may resort to some of the previously published method. For the sake of comparison, for the particular case of static blind node we will compare our approach against the method previously proposed in [7], hereafter referred as "range-based DTDOA". A schematic workflow of this method is given in Fig. 5. A key point of this method is represented by the the estimation of pseudo-ranges (or equivalently: distance differences) between the blind node and the anchors, hence the term "range-based". Timestamps are used to estimate pseudo-ranges, and the latter are then used to estimate positions. This strategy has two drawbacks. First, it does not extend easily to the case of moving node, where the range (distance) between the blind node and each anchor varies: in this case, one would need to model *each individual range variable with a time-varying function* (e.g. a polynomial). This approach, similar to the method considered in [10], would greatly increase the dimensionality of the search space.

Another disadvantage is that the range-based approach breaks the estimation process from timestamp measurements to final position estimate by introducing a layer of intermediate variables, namely the pseudo-ranges. This represents an approximation to the original problem that comes at the cost of a certain loss of precision, as shown below.

6 Simulation Results

6.1 Scenario

The blind node lies within a squared area of interest of size 250×250 meters, at the (known) fixed height of $p_z = 1.5$ meters. For each trial, the initial blind node position is extracted randomly within the area of interest

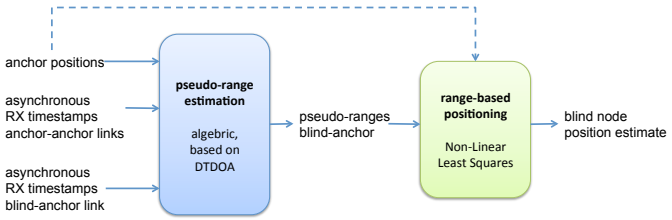

Figure 5. Workflow of range-based DTDOA method [7].

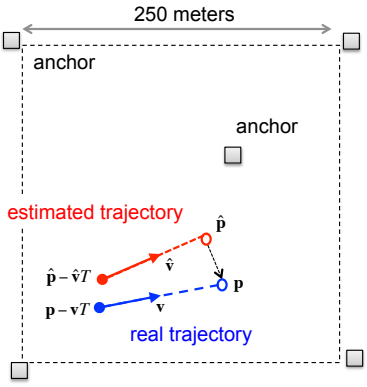

Figure 6. Reference topology with $N = 5$ anchors.

and its speed is set randomly between 3 and 6 m/s. The moving direction is random, with the constraint of ensuring that the final point remains within the area of interest. We consider $N = 5$ anchors placed as depicted in Fig. 6 at the fixed height of 4 meters. The relative frequency offset and temporal offset of each node clock are extracted randomly in the range $[-40, +40]$ ppm and $[0, 100]$ ms, respectively. Timestamp measurement errors are i.i.d. uniformly distributed in $[-\tau, +\tau]$ with $\tau = 25$ ns (corresponding to 20 MHz sampling rate). The reception of a given packet at a generic anchor occurs with probability $1 - \lambda$ independently from other reception events, λ denoting the packet loss probability. During the observation period of duration $T = 10$ s, each anchor node emits $B = 10$ beacons, while the blind node emits $M = 40$ packets.

6.2 A first look at numerical resolution cost

For this work, all non-linear minimisation instances were implemented in Matlab© with the general purpose function `fminunc`. The built-in solver uses a trust-region method. In all our instances the analytic gradient was provided explicitly. The tolerance parameters and the initialisation point were set to the same values for all estimators. As expected based on the discussion above, in each trial all estimators always converge to the same solution, however they do so through different search paths. Recall that the TOA form (12) has a larger dimensionality than TDOA/S-TOA, with $K+M$ total variables instead of only K due to the presence of the packet transmission times as (additive) nuisance variables. Therefore, while both form eventually lead to the same solution

This article has been accepted for publication in a future issue of this journal, but has not been fully edited. Content may change prior to final publication. Citation information: DOI 10.1109/TMC.2018.2792443, IEEE Transactions on Mobile Computing

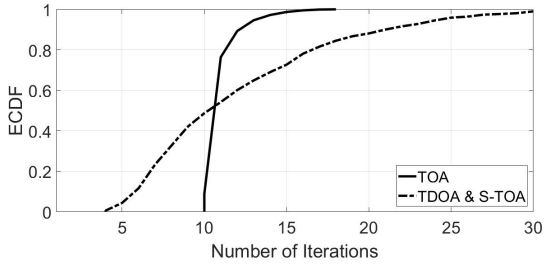

Figure 7. Number of iterations for a sample scenario.

(strong equivalence), the number of numerical iterations is not necessarily the same.

Fig. 7 reports the distribution of the number of iterations needed to solve each estimator form in the simulation scenario described in Sec. 6.1, with asynchronous anchors and 20% packet loss, for 1000 Monte Carlo trials. As expected, the curves for S-TOA and TDOA overlap exactly, since the two objective functions (hence their gradients) are equal across the whole search space, therefore the numerical gradient-descendent procedure follows exactly the same search path for the two estimators. A bit surprisingly, it appears that in 40% of the trials TOA converges with *less* iterations than TDOA/S-TOA, reminding us that convergence speed depends not only on the size of the search space, but also on the shape of the objective function to be minimized.

6.3 Comparison with DTDOA for static emitter

We start comparing the accuracy of the proposed method against the range-based DTDOA method from [7], in the particular case of a static blind node. In Fig. 8 we report the error distribution for the three methods described earlier in Sec. 5.4 for the case of $\lambda = 0$. In fact, the lossless scenario is the most favourable case for the DTDOA method, wherein input measurements are built from the difference of four reception timestamps associated to *packet pairs*, and is therefore more sensitive to packet loss. Despite the favourable scenario, the range-based DTDOA method performs markedly worse than the direct TOA/TDOA methods proposed in this work. Note also that the accuracy of the Dynamic TOA/TDOA approach is very close to that of the Static TOA/TDOA.

6.4 Results with moving node

In order to compare the estimated and actual trajectories we shall consider the following error metrics:

- The position error $\epsilon_p = \|\hat{\boldsymbol{p}} - \boldsymbol{p}\|$ given by the distance between the estimated and actual final positions.
- The speed error $\epsilon_{speed} = \|\hat{\boldsymbol{v}}\| - \|\boldsymbol{v}\|$ given by the difference between the estimated and actual speed.
- The heading error $\epsilon_{angle} = \arccos \frac{\hat{\boldsymbol{v}}^T \boldsymbol{v}}{\|\hat{\boldsymbol{v}}\| \|\boldsymbol{v}\|}$ given by the absolute angle between the estimated and actual velocity vectors.

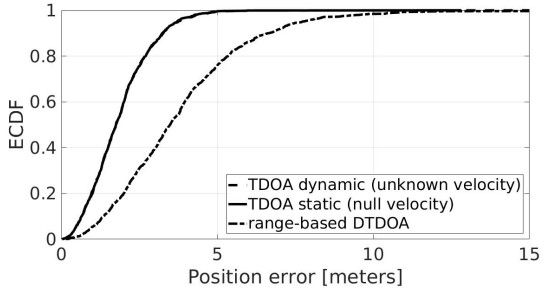

Figure 8. Final localisation error for static blind node (asynchronous scenario with $\lambda = 0$).

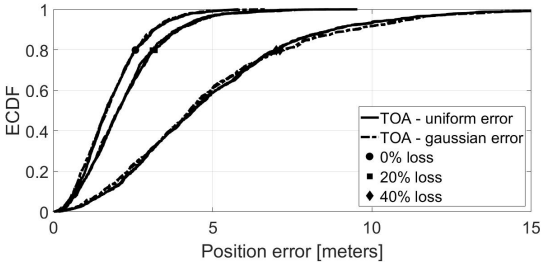

(a) Asynchronous anchors

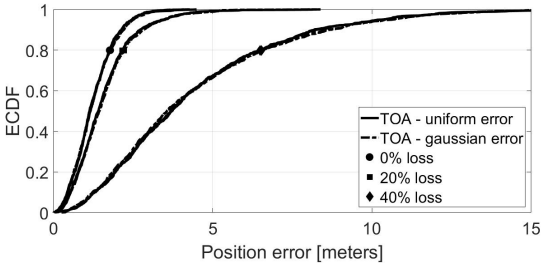

(b) Synchronous anchors

Figure 9. ECDF of absolute position error ϵ_p for different loss probability $\lambda \in \{0, 0.2, 0.4\}$.

In Fig. 9(a) we report the distribution of the position error ϵ_p obtained for different values of packet loss intensities $\lambda \in \{0, 0.2, 0.4\}$. To validate our implementation, for each individual Monte Carlo trial we run all three estimators — TOA, TDOA and S-TOA — and verify that the final solution was always exactly the same for all three methods (each curve in Fig. 9(a) is actually the superposition of three perfectly overlapping curves).

For each value of λ, we considered two distinct distributions for the input measurement error: uniform in $[-\tau, +\tau]$ and gaussian with same variance $\sigma_e^2 = \frac{\tau^2}{3}$, for $\tau = 25$ ns. Fig. 9(a) shows that the final error distribution is similar in both cases, confirming the practical validity of the LS solution also for non-gaussian input noise.

As expected, Fig. 9(a) shows that increasing the packet loss implies a certain loss of information, and therefore lower estimation accuracy. While for moderate packet loss such degradation remains contained (compare the curves for $\lambda = 0$ and $\lambda = 0.2$), it becomes noticeable for higher loss levels. This is clearly to be expected,

This article has been accepted for publication in a future issue of this journal, but has not been fully edited. Content may change prior to final publication. Citation information: DOI 10.1109/TMC.2018.2792443, IEEE Transactions on Mobile Computing

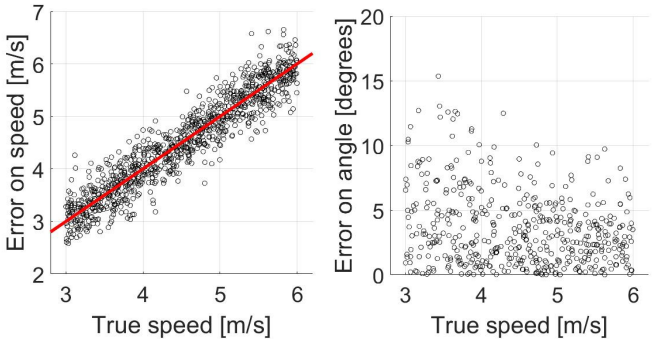

Figure 10. Error on speed (left) and angle (right) of the estimated velocity versus true speed (asynchronous anchors, 20% packet losses).

considering that the loss level has a direct impact on the number of data points used for the estimation. This effect is further amplified by the discarding of single-received packets in the pre-filtering stage.

The curves in Fig. 9(a) are obtained in the case of asynchronous anchors (with independent clocks) after estimating the clock error terms with the procedure described in Sec. 3 and adjusting the reception timestamps accordingly. It is interesting to compare these results with Fig. 9(b), reporting what is obtained in the ideal scenario where all receiving anchors are perfectly synchronised *ex ante* to a common clock, and therefore no timestamp adjustment is needed. Comparing the corresponding curves in Fig. 9(a) and Fig. 9(b) we observe that the penalty due to the imperfect recovery of clock synchronisation is pretty small, less than half meter in this scenario. These results indicate that synchronisation, if not provided natively by the system *on the node clocks*, can be effectively achieved in post-processing *on the data*, based on timing measurements from reference transmitters (not necessarily cooperative). On the other hand, the penalty due to high packet loss is much higher, since high packet loss translates directly into loss of data.

From a system engineering point of view, our results indicate that it would be more convenient, for the sake of localisation accuracy, to invest in better reception, with smarter receivers that are able to reduce packet loss (lower λ) and at the same time increase timing accuracy (reduce measurement noise variance), rather than investing in building additional synchronisation infrastructure.

Figure 10 reports the error on the estimated velocity, separately for modulus (speed) and absolute angle, versus the true speed of the blind node. It can be seen that in the tested scenario the speed can be estimated within ± 0.5 m/s, and that the speed error is rather independent from the actual speed. The estimated velocity direction was mostly within $\pm 10^\circ$ off the actual direction.

6.5 Comparison with Cramér-Rao Bound

In this section we derive the Cramér-Rao Bound (CRB) for the localisation problem assuming perfect synchronisation and gaussian measurement noise with variance $VAR(\tilde{e}_{nm}) = \sigma^2 = c^2\sigma_\varepsilon^2$. From the negative log-likelihood $\ell(\boldsymbol{z}, \boldsymbol{t})$ given in (11) we derive the Fisher Information Matrix (FIM) $\boldsymbol{F}$ by particularising the general Slepian-Bangs formula (see [24] and [25, Chapter 3]):

$$\boldsymbol{F} = \frac{1}{\sigma^2}\left[\begin{array}{c|c} \boldsymbol{B}_{[4\times 4]} & \boldsymbol{A}_{[4\times M]} \\ \hline \boldsymbol{A}^T_{[M\times 4]} & \boldsymbol{N}_{[M\times M]} \end{array}\right].$$

The matrix $\boldsymbol{N}_{[M\times M]} = \mathrm{diag}\{N_1, \ldots, N_M\}$ is diagonal with the mth element equal to the number of anchors N_m that have captured packet m. The generic element of $\boldsymbol{A}$ is given by $a_{km} = \sum_{n\in\mathcal{A}_m} \frac{\partial d_{nm}(\boldsymbol{z})}{\partial z_k}$ for $k = 1, \ldots, 4$ and $m = 1, \ldots, M$. The generic element of the symmetric square matrix $\boldsymbol{B}$ is given by $b_{k_1k_2} = b_{k_2k_1} = \sum_{m=1}^{M}\sum_{n\in\mathcal{A}_m} \frac{\partial d_{nm}(\boldsymbol{z})}{\partial z_{k_1}} \cdot \frac{\partial d_{nm}(\boldsymbol{z})}{\partial z_{k_2}}$ for $k_1, k_2 = 1, \ldots, 4$. The diagonal elements reduce to $b_{kk} = \sum_{m=1}^{M}\sum_{n\in\mathcal{A}_m}\left(\frac{\partial d_{nm}(\boldsymbol{z})}{\partial z_{k_1}}\right)^2$. Recalling the definition (9) of the distance term, the partial derivatives develop as:

$$\begin{aligned}
\frac{\partial d_{nm}(\boldsymbol{z})}{\partial z_1} &= \frac{\partial d_{nm}(\boldsymbol{z})}{\partial p_x} = \frac{p_x - v_x\cdot(T - \overline{R'_m}) - x_n}{d_{nm}(\boldsymbol{z})} \\
\frac{\partial d_{nm}(\boldsymbol{z})}{\partial z_2} &= \frac{\partial d_{nm}(\boldsymbol{z})}{\partial p_y} = \frac{p_y - v_y\cdot(T - \overline{R'_m}) - y_n}{d_{nm}(\boldsymbol{z})} \\
\frac{\partial d_{nm}(\boldsymbol{z})}{\partial z_3} &= \frac{\partial d_{nm}(\boldsymbol{z})}{\partial v_x} = -\frac{\partial d_{nm}(\boldsymbol{z})}{\partial p_x}(T - \overline{R'_m}) \\
\frac{\partial d_{nm}(\boldsymbol{z})}{\partial z_4} &= \frac{\partial d_{nm}(\boldsymbol{z})}{\partial v_y} = -\frac{\partial d_{nm}(\boldsymbol{z})}{\partial p_y}(T - \overline{R'_m}).
\end{aligned} \tag{18}$$

The CRB is given by the inverse of FIM $\boldsymbol{S} \stackrel{\text{def}}{=} \boldsymbol{F}^{-1} = \sigma^2\left[\begin{array}{c|c} \boldsymbol{B} & \boldsymbol{A} \\ \hline \boldsymbol{A}^T & \boldsymbol{N} \end{array}\right]^{-1} = \sigma^2\left[\begin{array}{c|c} \left(\boldsymbol{B} - \boldsymbol{A}\boldsymbol{N}^{-1}\boldsymbol{A}^T\right)^{-1} & \ldots \\ \hline \ldots & \ldots \end{array}\right]$. The upper four diagonal elements of $\boldsymbol{S}$, denoted by $s_{kk},\ k = 1, \ldots, 4$, represent lower bounds to the variance of the final estimates for the four variables of interest, respectively $\hat{p}_x, \hat{p}_y, \hat{v}_x$ and $\hat{v}_y$. For each variable, we compare in Fig. 11 the Mean Square Error (MSE) obtained with our estimation method across 1000 Monte Carlo trials to the corresponding CRB value s_{kk}. The curves were obtained in a fixed sample topology considering different numbers of source packets $M \in [6, \ldots, 40]$. The "*sinch.*" data points were obtained for the ideal case of perfectly synchronised anchors, while the "*asinch.*" data were obtained for asynchronous anchors, by running the data synchronisation procedure described in Sec. 3 with $B = 40$ before the localisation procedure. As expected, increasing M reduces the estimation error. From Fig. 11 we observe that the precision of our method is very close to the theoretical bound, and that the penalty due to the imperfect recovery of clock synchronisation is small.

7 Experimental Results in WiFi Testbed

In order to validate the proposed solution in a real environment we have performed experiments in a testbed deployed at University of Brescia and composed of commercial WiFi devices. We ran three different rounds of experiments with different modulation schemes and

This article has been accepted for publication in a future issue of this journal, but has not been fully edited. Content may change prior to final publication. Citation information: DOI 10.1109/TMC.2018.2792443, IEEE Transactions on Mobile Computing

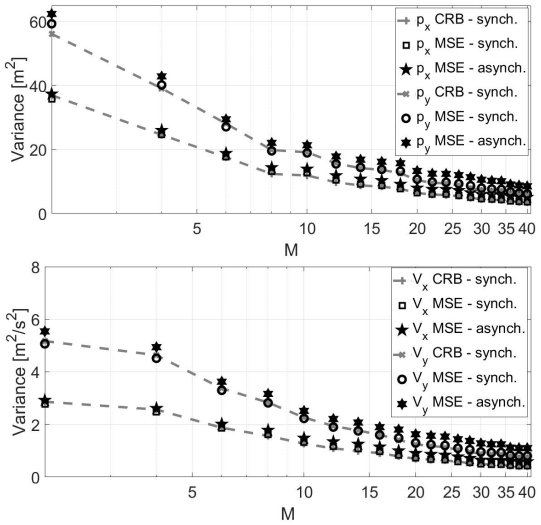

Figure 11. Comparison of the empirical MSE and theoretical CRB for position (top) and velocity (bottom) variables for 1000 Monte Carlo trials on a sample topology.

timestamp resolution values. The first two rounds of experiments were based on IEEE 802.11b transmission with DSSS modulation and timestamp resolution of 45.4 ns. The third round of experiments was based on IEEE 802.11g transmission with OFDM modulation, and a refined timing resolution of approximately 10 ns. All experiments were conducted in an open outdoor area (garden) with all nodes in full Line-of-Sight (LOS) conditions. The actual node positions (ground truth) were measured manually with an accuracy of 2-3 centimetres.

7.1 Testbed setup with IEEE 802.11b DSSS radios and hardware timestamps

The testbed deployment consists of multiple fixed devices (anchors) and one mobile device acting as blind node. The nodes are programmed to send UDP packets at a configurable average rate. Channel access at the MAC layer is performed using the standard DCF protocol with a Contention Window of 15 slots.

All nodes are set to transmit in IEEE 802.11b mode with DSSS modulation and datarate of 2 Mb/s on a single channel. For these tests we used WRT54GL devices from Linksys, i.e., the same used in [7]. These devices are cheap and run a very robust OpenWRT distribution based on Linux Kernel 2.6.32. Most importantly, their Network Interface Card (NIC) is compatible with OpenFWWF [26], an open source firmware that replaces the original binary-only software from Broadcom and has been widely used as research platform [27], [28]. The modified OpenFWWF firmware[4] allows to extract the hardware timestamp (according to the local clock) corresponding to the last sample of the incoming packet. Although the CPU clock runs at 88 MHz, the last two

4. The OpenFWWF firmware used for these experiments is publicly available at http://netweb.ing.unibs.it/openfwwf/localisation.

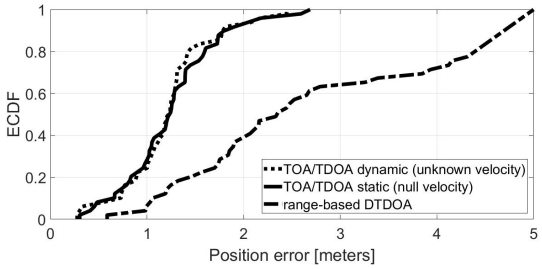

Figure 12. Experimental performances of different localisation schemes for static node.

bits of every timestamp are non-informative, since the timing resolution is limited by the sampling rate of $F_s = 22$ MHz. In summary, we obtain timestamps with a resolution of $T_s = 1/F_s = 45.4$ ns, corresponding to 13.6 meters at speed of light.

Experiment #1: comparison with range-based DTDOA localisation for a static node

In the first set of experiments we aim at comparing the accuracy of the proposed estimators with the range-based DTDOA method described earlier in [7], for the particular scenario of static blind node. For these tests we have considered three different topologies consisting of 6 anchors and one (static) blind node placed in a rectangular area of 15 $\times$ 10 meters. For each topology we collected 18 different datasets by repeating the measurement in different (non overlapping) time intervals. In this way we end up with a total of 54 different trials. The duration of each trial was 3 s, and each node (anchor and blind) was set to transmit in IEEE 802.11b mode at the average rate of 56 packets/s.

The ECDF of the absolute error plotted in Fig. 12 confirms that our direct resolution methods (range-free) beats the range-based DTDOA method. The Dynamic and Static versions of our algorithms perform very similarly for the particular case of static blind node. These experimental results are in good agreement with the previous simulation results from Fig. 8.

Experiment #2: moving node

In this second set of experiments, we considered a fixed topology of 10 anchors. For each trial, a person was walking at approximately constant speed along a straight trajectory fully contained within the convex hull of the anchor nodes. Each individual trial lasts between 4 and 5 s. During each trial, each node (anchors and blind) was transmitting in IEEE 802.11b mode at the average rate of 56 packets/sec. In Fig. 13 we report the actual trajectory (ground truth, in blue continuous line) along with the final estimated trajectory (dashed red line) for some sample experiments. It can be seen that the estimation error remains below 1 meter.

This article has been accepted for publication in a future issue of this journal, but has not been fully edited. Content may change prior to final publication. Citation information: DOI 10.1109/TMC.2018.2792443, IEEE Transactions on Mobile Computing

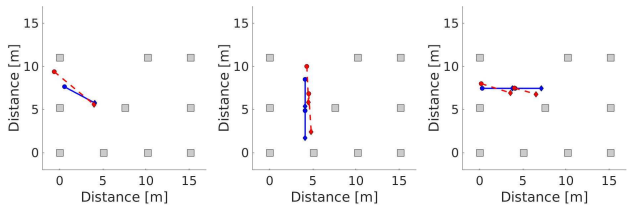

Figure 13. Sample results for IEEE 802.11b DSSS modulation and hardware timestamps. All anchors nodes serve both as receivers and reference transmitters. Actual trajectory (blue) vs. Estimated trajectory (red dotted).

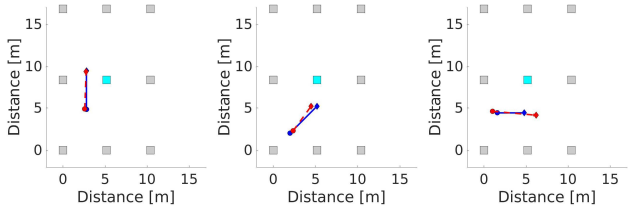

Figure 14. Sample results for IEEE 802.11g OFDM modulation and CSI-corrected timestamps). The central node ("pivot") serves as the single reference transmitter, while all other nodes act purely as receivers.

7.2 Testbed setup with IEEE 802.11g OFDM radios and refined timestamps

For the third round of experiments we turned all nodes to IEEE 802.11g mode with OFDM modulation and datarate of 6 Mb/s. For these experiments we have adopted a new prototype version of the OpenFWWF firmware that is able to report for each received packet also the Channel State Information (CSI), i.e., an estimate of the channel frequency response computed by the baseband processor on the basis of the 52-bits preamble of each packet. The baseband processor uses CSI to equalise the OFDM symbol, but this information can be used to improve the accuracy of TOA measurements by means of so-called Super-Resolution Algorithms [29]. This approach was recently adopted for WiFi [30] and LTE signals [31]. For this work we have implemented a procedure for timestamp correction based on CSI that is similar in spirit to the method proposed in [30], particularised for a single channel. In this way we were able to reduce the timing error down to ± 10 ns.

For this third round of experiments we have placed 9 fixed nodes in a regular 3×3 grid as shown in Fig. 14, plus one mobile device acting as blind node. Differently from the previous experiments, where each anchor was serving both as receiver and (reference) transmitter, in this round we assigned to each anchor a specialised role: the 8 external anchors were configured to serve purely as receivers, while the single central node (denoted as "pivot" node hereafter) serves as the single reference transmitter for the synchronisation phase.

Both the pivot and the blind node act purely as transmitters and do not cooperate to the localisation process. They are programmed to send UDP packets at the average rate of 9 packets/sec, a considerably lower value than the previous experiments. The TOA measurements (after CSI correction) collected by the receiving anchors for the packets transmitted during this period by the pivot and by the blind node are fed in input, respectively, to the synchronisation phase (3) and to the TOA estimator (12).

Experiment #3: moving node with refined timestamps

In Fig. 14 we report the actual and estimated trajectory for three sample experiments. The accuracy is roughly similar to the previous set of experiments, with midpoint errors below 1 meter. However this result was achieved with a much smaller number of packets compared to the previous experiments. In other words, the improved timing resolution gained with CSI correction allowed to achieve the same final accuracy with a considerably smaller number of more accurate measurements.

8 Related Work

To the best of our knowledge there is no solution in the literature that can be applied to the considered scenario, since all previously proposed methods fail to meet one or more of the system requirements (a)-(d) outlined earlier in Section 1. The vast majority of previous work on time-based localisation in asynchronous networks, including e.g. [10], [11], [12], [13], [14], [15], [16], [17], [32], [33] rely on the knowledge or tight control of transmission times in addition to reception times, and require some form of cooperation by the blind node. This applies particularly to the solutions based on two-way ranging [10], [34], [35]. Such methods can not be used to implement fully opportunistic localisation on top of legacy wireless systems without transmitter cooperation, and therefore can not be directly compared to our work. In [9], [36] the authors have considered nodes clock with zero frequency offset, effectively assuming "quasi-synchronous" scenario instead of "fully asynchronous" (following the taxonomy proposed in [11]) and static blind nodes, thus missing requirements (a) and (d). The only previous work considering all three conditions (a)-(c) are [7], [18] and more recently also [8], [19]. However, the resolution algorithms proposed in these papers were designed specifically for a static node (missing condition (d)) and cannot be extended easily to the case of a moving node. More specifically, the solutions proposed in [7], [18], [19] are range-based, i.e., they rely on the intermediate estimation of distances (or distance differences, or pseudo-ranges) between the blind node and the anchors, and therefore do not generalise straightforwardly to the case of moving nodes, where blind-anchor distances vary for each measurement. Similarly, the algorithms proposed in [8] rely on linear and/or semidefinite programming approximations of the core ML estimation problem tailored to the static scenario.

This article has been accepted for publication in a future issue of this journal, but has not been fully edited. Content may change prior to final publication. Citation information: DOI 10.1109/TMC.2018.2792443, IEEE Transactions on Mobile Computing

Some form of equivalence between TOA and TDOA formulations was noted in previous work, limited to the particular case of a static node. However, in most cases only "weak equivalence" was recognised, based on the comparison of the respective Cramer-Rao bounds (see e.g. [22] and references therein). The only explicit "strong equivalence" demonstration we found appears in [23, Theorem 2], but limited to linearised (approximated) versions of the TOA and TDOA estimators, and for the special case of a static node. To the best of our knowledge, no previous work has delved into the different facets of "equivalence" between TOA and TDOA (and S-TOA) for the general non-linear case.

Moving nodes and asynchronous clocks were considered earlier by Rajan et al. in [10]. There are however two important differences with our work. First, they consider a completely different set of system requirements, with measurement of transmission times (in addition to reception times) and two-way ranging. As such, their work cannot be applied to our system, where the transmitter is non-cooperative. Second, they follow a *range-based* approach, where each distance term (range) between the blind node and every individual anchor is modelled by a high-degree polynomial. In this way, even for the simplest scenario of a single blind node moving with linear trajectory, they need to introduce a large set of variables, equal to the number of anchors times the polynomial degree. Instead, our approach to model directly the instantaneous *position* of the blind node is much more parsimonious in the number of variables.

9 Conclusions and Future Work

In this work we have considered the problem of determining the (linear) trajectory parameters of a non-cooperative moving emitter based solely on the reception timestamps collected by a set of cooperative receivers (anchors). In the proposed scenario, data synchronisation can be achieved in post-processing, by estimating the clock error terms (offset and skew) of the receiving nodes from the timestamps associated to packets transmitted by one ore more (non-cooperative) reference sources, possibly but not necessarily coinciding with the receiving anchors. For the problem at hand, we have derived three different forms of Non-linear Least Squares estimators based exclusively on reception time measurements, and proved their equivalence.

From a system-level point of view, our results indicate that improving the *precision* of reception timestamps, i.e., reducing the variance of random timing errors, is much more important than battling against clock misalignment by means of costly node synchronisation infrastructure. In fact, if *node synchronisation* is not implemented in the system, *data synchronisation* can still be effectively achieved in post-processing, by leveraging cooperation between the receivers. This is because systematic clock errors can be easily estimated and compensated in post-processing. The main take-home message of our work is that engineers and system developers should *give priority to investing into better receiver implementations, to increase the precision of reception timestamps and reduce packet loss, rather than endowing the system with costly synchronisation infrastructure*.

One key aspect of the proposed method is the ability to exploit lossy measurements. Packets that are received by as few as two receivers can be fruitfully exploited by our method based on "tracing" the trajectory parameters along the whole (small) observation window, whereas alternative methods based on point-by-point localisation would require each individual packet to be received by no less than three (in 2D) or four (in 3D) receivers.

In the progress of this work we are investigating more robust variants of the TOA estimator against large errors, e.g., due to Non-Line-of-Sight propagation, by complementing the core estimator with pruning heuristics aimed at rejecting large errors, along the line of the procedures proposed e.g. in [7] ("slice and prune") and [30] ("clustering"). We remark that the NLOS problem affects *all* time-based localization methods, including the one proposed here as well as any previously proposed technique. Combating NLOS is a research problem per se, and NLOS countermeasures need to be tailored to the underlying localisation method. To date, NLOS filtering and mitigation strategies have been studied mostly for ranging and synchronous time-based methods, and to a less extent for TDOA [37], [38], [39]. An important direction for future work is to develop robust NLOS mitigation strategies for fully asynchronous schemes like the one presented here, and we hope that this contribution will motivate further research in this direction. Furthermore, we are investigating distributed privacy-preserving implementations of the proposed estimators.

References

[1] F. Ricciato, S. Sciancalepore, and G. Boggia. Tracing a linearly moving node from asynchronous time-of-arrival measurements. *IEEE Comm. Letters*, 20(9), June 2016.

[2] M. Alzantot and M. Youssef. Uptime: Ubiquitous pedestrian tracking using mobile phones. In *IEEE Wireless Comm. & Networking Conf. (WCNC'12)*, 2012.

[3] B. Bonne, A. Barzan, P. Quax, and W. Lamotte. Wifipi: Involuntary tracking of visitors at mass events. In *IEEE Int. Conf. on Pervasive Computing (ICPC'15)*, 2015.

[4] N. Bulusu et al. GPS-less Low Cost Outdoor Localization For Very Small Devices. *IEEE Personal Communications*, October 2000.

[5] A. Ahmed and A. Rajeswari. Intrusion detection in heterogeneous Wireless Sensor Networks with an energy efficient localization algorithm. In *Int. Conf. on Recent Trends in Inf. Tech.*, April 2012.

[6] R. Parker and S. Valaee. Vehicular node localization using received-signal-strength indicator. *IEEE Trans. on Vehicular Technologies*, 56(6), November 2007.

[7] N. Facchi *et al.* Emitter localisation from reception timestamps in asynchronous networks. *Computer Networks*, 88, September 2015.

[8] X. Wu and Z. Gu. A joint time synchronization and localization method without known clock parameters. *Pervasive and Mobile Computing*, 37, June 2017.

[9] O. Jean and A. Weiss. Passive localization and synchronization using arbitrary signals. *IEEE Trans. on Signal Proc.*, 62(8), 2014.

[10] R.T. Rajan and A. J Van der Veen. Joint ranging and synchronization for an anchorless network of mobile nodes. *IEEE Trans. on Signal Proc.*, 63(8), April 2015.

[11] Y. Wang, X. Ma, and G. Leus. Robust time-based localization in asynchronous networks. *IEEE Trans. on Signal Proc.*, 59(9), 2011.

[12] B. Liu, H Chen, Z. Zhong, and V. Poor. Asymmetrical round trip based synchronization-free localization in large-scale underwater sensor networks. *IEEE Trans. on Wireless Comm.*, 9(11), 2010.

[13] D. Zachariah, A. De Angelis, S. Dwivedi, and P. Haendel. Schedule-based sequential localisation in asynchronous wireless networks. *EURASIP Journal of Advances in Signal Proc.*, 2014.

[14] M. R. Gholami, S. Gezici, and E. G. Strom. Range-based sensor node localization in the presence of unknown clock skews. In *IEEE ICASSP*, 2013.

[15] T. Li, A. Ekpenyong, and Y.-F. Huang. Source localization and tracking using distributed asynchronous sensors. *IEEE Trans. on Signal Proc.*, 54(10), 2006.

[16] K. Yang, G. Wang, and Z. Luo. Efficient convex relaxation methods for robust target localization by a sensor network using time differences of arrivals. *IEEE Trans. on Signal Proc.*, 57(7), 2009.

[17] R. M. Vaghefi and R. M. Buehrer. Cooperative joint synchronization and localization in wireless sensor networks. *IEEE Trans. on Signal Proc.*, 63(14), July 2015.

[18] A. Nagy et al. Time-based localisation in unsynchronized wireless lan for industrial automation systems. In *IEEE Conf. on Emerging Technologies & Factory Automation (ETFA'11)*, 2011.

[19] D. Spano and Ricciato. F. Opportunistic time-of-arrival localization in fully asynchronous wireless networks. *Pervasive and Mobile Computing*, 37, June 2017.

[20] S. Lanzisera, D. Zats, and K. Pister. Radio frequency time-of-flight distance measurement for low-cost wireless sensor localization. *IEEE Sensors Journal*, 11(3), March 2011.

[21] K. Miller. On the inverse of the sum of matrices. *Mathematics Magazine*, 54(2), March 1981.

[22] R. Kaune. Accuracy studies for tdoa and toa localization. In *15th Int'l Conf. on Information Fusion (FUSION)*, 2012.

[23] D.-H. Shin and T.-K. Sung. Comparisons of error characteristics between toa and tdoa positioning. *IEEE Trans. on Aerospace and Electronic Systems*, 38, 2002.

[24] O. Besson and Y. Abramovich. On the fisher information matrix for multivariate elliptically contoured distributions. *IEEE Signal Proc. Letters*, 20(11), 2013.

[25] Steven Kay. *Fundamentals of Statistical Signal Processing, Volume I: Estimation Theory*. Prentice Hall, 1993.

[26] F. Gringoli and L. Nava. Openfwwf: Open firmware for wifi networks. available at http://www.ing.unibs.it/openfwwf.

[27] P. Salvador et al. Voipiggy: Analysis and implementation of a mechanism to boost capacity in ieee 802.11 wlans carrying voip traffic. *IEEE Trans. on Mobile Computing*, 13(7), 2014.

[28] D. Berger et al. Friendly jamming on access points: Analysis and real-world measurements. *IEEE Trans. on Wireless Comm.*, 15(9), Sept. 2016.

[29] X. Li and K. Pahlavan. Super-resolution toa estimation with diversity for indoor geolocation. *IEEE Trans. on Wireless Comm.*, 3(1), January 2004.

[30] J. Xiong, K. Sundaresan, and K. Jamieson. Tonetrack: Leveraging frequency-agile radios for time-based indoor wireless localization. In *ACM MobiCom*, 2015.

[31] M. Driusso and *et al.* Vehicular position tracking using LTE signals. *IEEE Trans. on Vehicular Technology*, July 2016. In press.

[32] R. M. Vaghefi and R. M. Buehrer. Asynchronous time-of-arrival-based source localization. In *IEEE ICASSP*, 2013.

[33] R. Kim and T. Ha. Tdoa localization for wireless networks with imperfect clock synchronization. In *IEEE ICOIN*, 2014.

[34] A. Marcaletti, M. Rea, D. Giustiniano, V. Lenders, and A. Fakhreddine. Filtering noisy 802.11 time-of-flight ranging measurements. In *ACM CoNEXT'14*, 2014.

[35] A. Fakhreddine, D. Giustiniano, and V. Lenders. Evaluation of self-positioning algorithms for time-of-flight based localization. In *WiOpt'16*, 2016.

[36] A. Coluccia, F. Ricciato, and G. Ricci. Positioning based on signals of opportunity. *IEEE Comm. Letters*, 18(2), February 2014.

[37] I. Guvenc and C. C. Chong. A survey on toa based wireless localization and nlos mitigation techniques. *IEEE Comm. Surveys & Tutorials*, 11(3), 2009.

[38] R. M. Vaghefi, J. Schloemann, and R. M. Buehrer. Nlos mitigation in toa-based localization using semidefinite programming. In *IEEE WPNC*, 2013.

[39] S. Hara et al. Analysis on toa and tdoa location estimation performances in a cellular system. In *IEEE ICC*, June 2011.

Fabio Ricciato Fabio Ricciato received the Ph.D. in 2003 from University La Sapienza, Italy. In 2004 he joined the Telecommunications Research Center Vienna, first as Senior Researcher and then as Key Researcher. Between 2007 and 2013 he was Assistant Professor at the University of Salento, Italy, and later served as Head of Business Unit at the Austrian Institute of Technology. He is currently professor at the Faculty of Computer and Information Science, University of Ljubljana, Slovenia. His research interests include radio localisation and Software-Defined Radio.

Savio Sciancalepore is currently PhD Student at Politecnico di Bari, Italy. He has obtained his bachelor and master degrees in 2011 and 2013 in Telecommunications Engineering. He is IEEE Student Member since August 2014. He is involved in the EU H2020 project symbIoTe. His major research interests are: Internet of Things (IoT) and Machine-to-Machine (M2M) and wireless localisation techniques.

Francesco Gringoli received the Laurea degree in telecommunications engineering from the University of Padua, Italy, in 1998 and the Ph.D. degree in information engineering from the University of Brescia, Italy, in 2002. Since 2005, he has been an Assistant Professor of Telecommunications in the Dept. of Information Engineering at the University of Brescia, Italy. He started the OpenFWWF Project in 2009. He is a senior member of the IEEE.

Nicolò Facchi is a postdoc research fellow at the Department of Information Engineering and Computer Science of the University of Trento, Italy. He received the Ph.D in Telecommunication Engineering from the University of Brescia in 2016. His current research interests include real time video streaming and overlay management in P2P networks and performance evaluation of medium access control in Wireless LANs.

Gennaro Boggia (S'99 – M'01 – SM'09) received, a Ph.D. in Electronics Engineering in March 2001. Since 2002 he is with the Dep. of Electrical and Information Engineering of Politecnico di Bari, where he is currently Associate Professor. His research interests span the fields of Wireless Networking, Network Security, Cellular Communication, Information Centric Networking, Internet of Things, Protocol stacks for industrial applications, Internet measurements, Network Performance Evaluation. He serves as Associate Editor for the Wireless Networks and ETT journals.